FOSSEE CFD-OpenFOAM Semester Long Internship
Spring 2026

on

Numerical Simulation of an Undulatory NACA0012 Hydrofoil using Overset Mesh

Keshav Poudel[1], Parees Palkar[2], and Chandan Bose[3]

[1]Alumnus, Department of Mechanical and Aerospace Engineering, Pulchowk Campus, Institute of Engineering, Tribhuvan University, Nepal
[2]Research Assistant, CFD FOSSEE, IIT Bombay
[3]Assistant Professor, Aerospace Engineering, College of Engineering and Physical Sciences, The University of Birmingham

July 9, 2026

Synopsis

This report presents a numerical study on the propulsive performance of an undulating NACA0012 hydrofoil using the Overset Mesh framework in OpenFOAM-v2412. The study employs a hybrid swimming kinematics model combining an anguilliform wavelength ($\lambda^* = 0.8$) with a carangiform quadratic amplitude envelope peaking at 0.10 m at the trailing edge. A parametric sweep was performed across Strouhal numbers from $St = 0.20$ to 0.70. The numerical model captures the drag-to-thrust transition near $St \approx 0.30$, and the mean thrust coefficient (C_{Tm}) trends show a close match against the reference data. The propulsive efficiency peaks at $\eta_p = 49.18\%$ for $St = 0.60$ and decreases to 47.74% at $St = 0.70$, exhibiting the characteristic efficiency hump curve.

Keywords: Undulatory Propulsion, Overset Mesh, OpenFOAM, NACA0012, Strouhal Number, Reverse von Kármán Street.

1 Introduction

Bio-inspired underwater propulsion offers an alternative to traditional propellers, providing high maneuverability and low acoustic signatures. This study focuses on the undulatory mode, which is utilized for efficient cruising in marine species. These species use unsteady, oscillatory, and undulatory motions to generate thrust. The motion involves a traveling wave that propagates along the body, increasing in amplitude towards the tail.

The primary motivation for this research is to investigate undulatory motion using numerical methods. Standard rigid-body mesh motion methods often encounter limitations at high amplitudes due to cell distortion. This study addresses this issue using the Overset (Chimera) Mesh framework. By decoupling the motion of the foil from the background domain, grid quality is preserved during large-amplitude movements.

2 Computational Methodology

2.1 Geometry and Mesh Generation

The spatial discretization of the domain utilizes a multi-block overset (Chimera) framework, consisting of a stationary background domain ($X \in [-5, 11]$ m, $Y \in [-5, 5]$ m) and a moving component domain enclosing the NACA0012 hydrofoil. Both domains were discretized using `blockMesh` and refined with `snappyHexMesh`. To minimize interpolation errors at the overlapping boundary, a 1:1 cell-size matching strategy was enforced, standardizing the cell size Δx at the overset interface to exactly 0.025 m. The resulting mesh consists of 168,818 cells (156,040 in the background and 12,778 in the component domain). Figure 1 shows the domain boundaries, Figure 2 shows the grid, and Figure 3 illustrates the overset cell classifications.

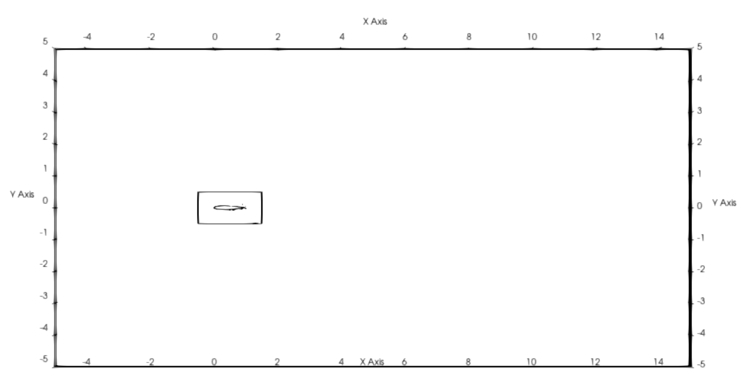

Figure 1: Schematic representation of the computational domain boundaries.

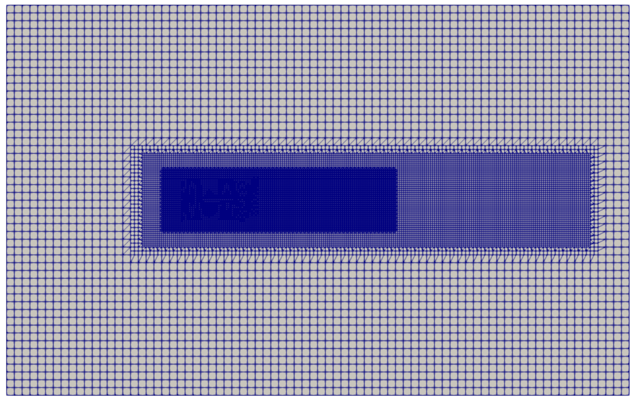

Figure 2: Multi-block overset grid configuration showing the component and background meshes.

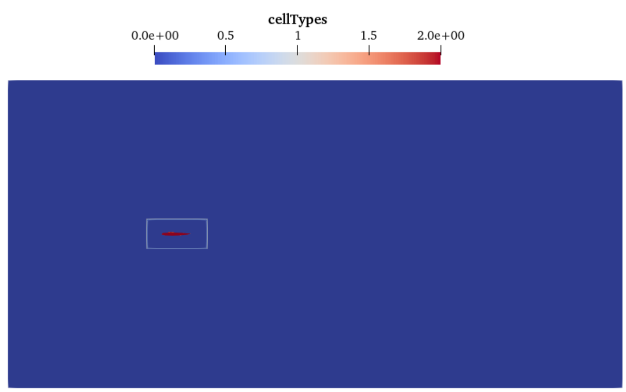

Figure 3: Visualisation of dynamic overset cell classification, highlighting the calculated (active), interpolated (fringe), and hole (inactive) cells.

2.2 Numerical Setup and Kinematics

2.2.0.1 Solver and Numerics

Simulations were performed using the overset-compatible PIMPLE solver `overPimpleDyMFoam` in OpenFOAM-v2412. The pressure system was resolved using the `PBiCGStab` solver with a `DILU` preconditioner to prevent multi-grid instabilities. Temporal discretization was handled using a second-order backward implicit scheme. The time step was set to $\Delta t = 0.0005$ s initially, and subsequently increased to $\Delta t = 0.001$ s once stable.

2.2.0.2 Kinematics and Coded Motion

The undulatory motion is defined by the traveling wave equation $y(x,t) = A(x)\sin(kx - \omega t)$ with a quadratic amplitude envelope $A(x) = 0.02 - 0.08x + 0.16x^2$ m, where $k = 2\pi/\lambda^*$ (wavelength $\lambda^* = 0.8$) and $\omega = 2\pi f$. A custom C++ dynamic mesh solver translates the entire overset domain as a rigid body with the mid-chord heave displacement (y_{heave}). The local mesh displacement is blended from full undulatory motion at the foil surface to pure heave at the overset boundaries using a distance-based weighting factor $w = 1 - (y - y_t)/(y_{max} - y_t)$, with a cosine-based falloff function smoothing the boundaries. A startup ramp is applied during the first 0.1 s.

2.2.0.3 Boundary and Initial Conditions

Boundary conditions for velocity and pressure are summarized in Table 1. The flow is initialized with a uniform velocity $U = 1.0$ m/s, with turbulence properties specified at a turbulence intensity of 1% for $Re = 5000$.

Table 1: Summary of Boundary Conditions for Velocity and Pressure

Boundary Patch	Velocity (U)	Pressure (p)
Inlet	`fixedValue` (1 0 0)	`zeroGradient`
Outlet	`zeroGradient`	`fixedValue` 0
Foil Surface	`movingWallVelocity`	`zeroGradient`
Top/Bottom Walls	`slip`	`zeroGradient`
Overset Patches	`overset`	`overset`

3 Results and Discussions

3.1 Validation

The numerical results were validated against the reference data of Thekkethil et al. [1]. Figure 4 shows a side-by-side comparison of both the mean thrust coefficient (C_{Tm}) and the RMS lift coefficient ($C_{L,rms}$) across the range of Strouhal numbers. The present CFD results match the benchmark trends, capturing the drag-to-thrust transition near $St \approx 0.30$ and the rising lift oscillations. A minor numerical offset is observed relative to the reference curves. This arises from the different numerical methodologies: the reference paper uses an immersed boundary method, whereas the present work uses the Overset (Chimera) Mesh framework. The observed offsets are therefore attributed to differences in discretization and interface treatment between the two solvers, while the overall physical trends are reproduced.

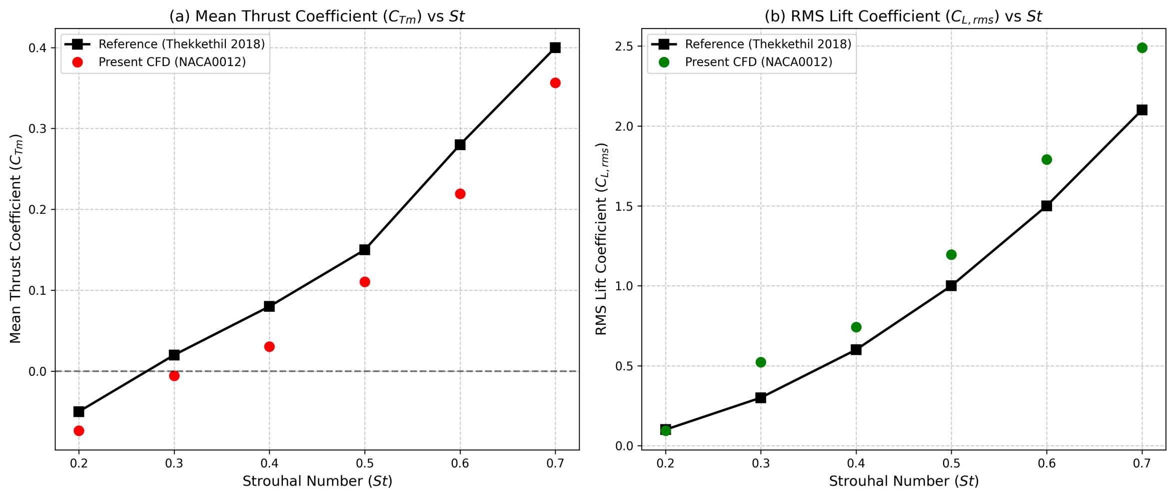

Figure 4: Validation: Comparison of (a) Mean Thrust Coefficient (C_{Tm}) and (b) RMS Lift Coefficient ($C_{L,rms}$) vs Strouhal Number (St) against reference data [1].

3.2 Detailed Analysis of the Flow Field and Dynamic Forces

To analyze the physical mechanisms of propulsion, the flow fields and force dynamics across different Strouhal numbers were investigated. The transition from a drag-producing wake to a thrust-producing wake is visualized in Figure 5. At $St = 0.2$, the wake exhibits a standard von Kármán street, generating a velocity deficit. At $St = 0.4$, the vortices begin to align, and by $St = 0.6$, a clear Reverse von Kármán street emerges, inducing a strong downstream propulsive jet (Figure 6).

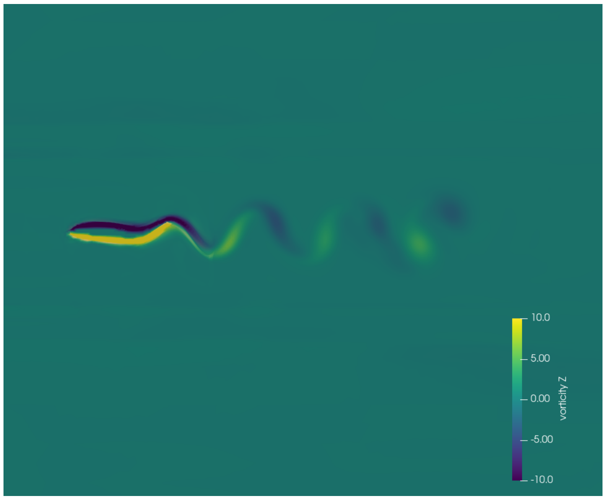

(a) $St = 0.2$

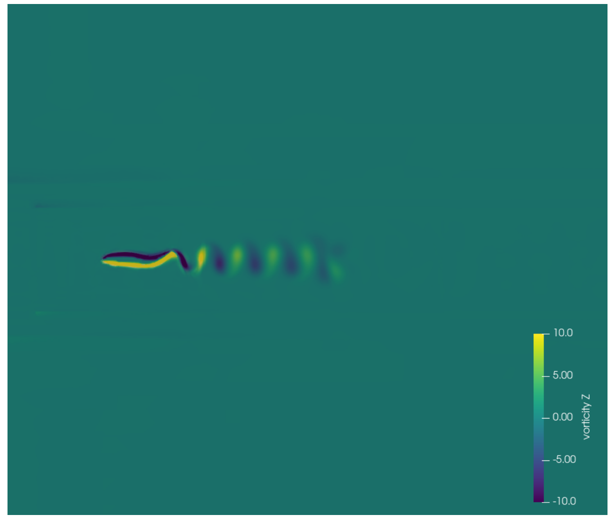

(b) $St = 0.4$

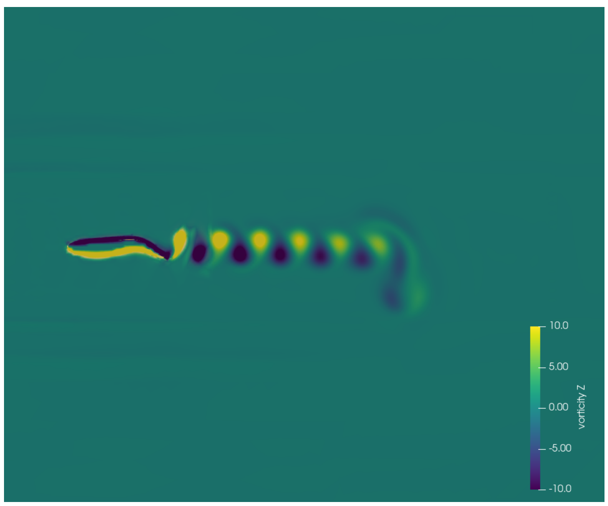

(c) $St = 0.6$

Figure 5: Instantaneous Z-vorticity (ω_z) field demonstrating the transition from a drag-producing standard von Kármán street ($St = 0.2$) to a thrust-producing Reverse von Kármán street ($St = 0.6$).

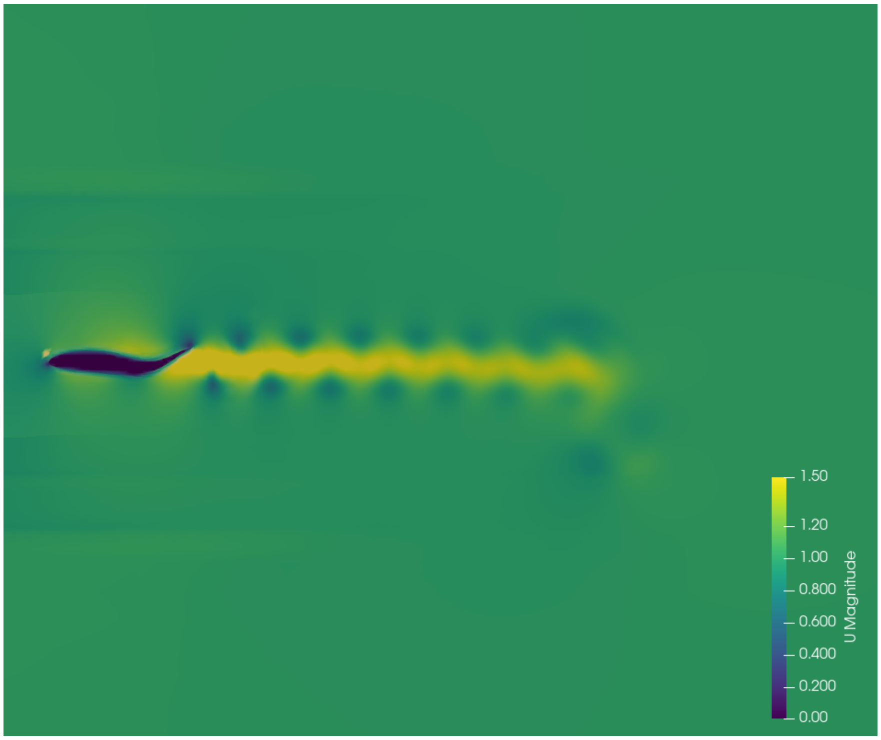

Figure 6: Instantaneous velocity magnitude ($|U|$) contour showing the propulsive jet flow in the wake.

The vorticity field (Figure 5) displays a clear Reverse von Kármán vortex street at higher Strouhal numbers, where counter-rotating vortex pairs are shed into the wake. The rotation direction of these vortices induces a strong downstream jet along the centerline, which is qualitatively represented by the high-velocity core ($|U| > 1.2$ m/s) in Figure 6. This jet is the physical source of thrust generation.

Quantitatively, for this representative $St = 0.6$ case, the numerical simulation recorded a mean thrust coefficient of $C_{Tm} = 0.2192$ and an RMS lift coefficient of $C_{L,rms} = 1.7910$. Similar quantitative evaluations were performed for the other simulated Strouhal numbers to obtain the comparative results.

Figure 7 illustrates the non-dimensional time-history of the lift and thrust coefficients over the final three steady-state cycles for the $St = 0.6$ case. The lift coefficient oscillates symmetrically, matching the kinematic period, while the thrust coefficient oscillates at twice the heave frequency, confirming that forward thrust is generated during both the upstroke and downstroke.

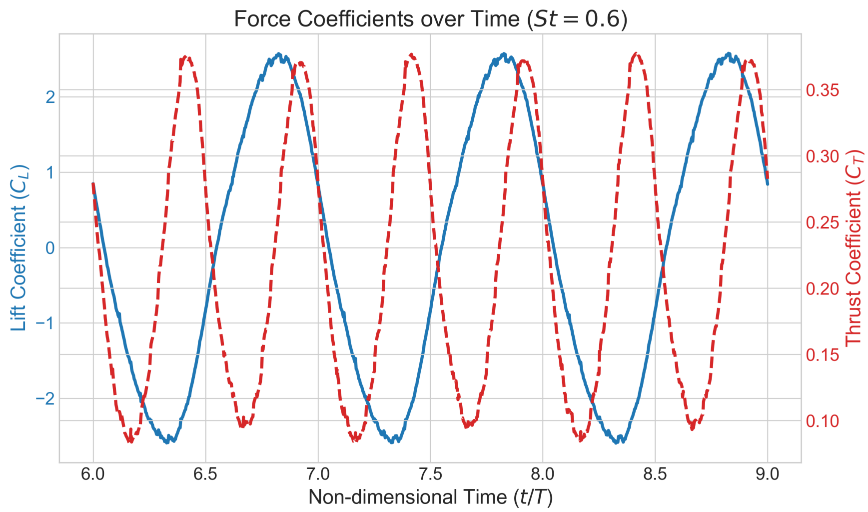

Figure 7: Instantaneous Force Coefficients over the final three cycles ($St = 0.6$).

The stability of the propulsive cycle is further demonstrated by the phase portrait (Figure 8), which plots C_L against C_T for a single period. The perfectly closed "figure-eight" limit cycle at $St = 0.6$ confirms that the simulation has achieved a fully converged, periodic steady state devoid of numerical transients.

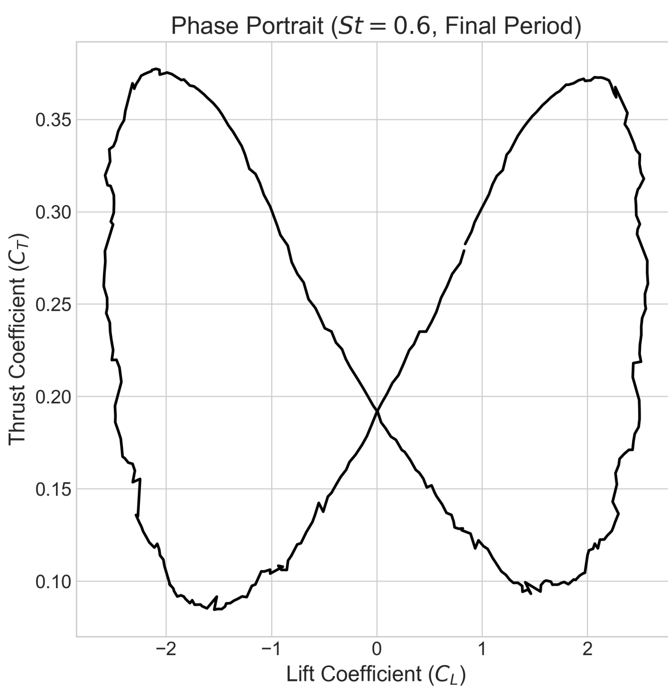

Figure 8: Phase portrait of Lift vs Thrust coefficient for a single cycle ($St = 0.6$).

To quantify the underlying flow physics responsible for this thrust, the downstream wake velocity profile was extracted at three stations ($x/c = 2, 4$, and 6) for the $St = 0.6$ case, as shown in Figure 9. A clear momentum surplus is observed at the centerline ($y/c \approx 0$), proving the existence of a high-velocity jet induced by the Reverse von Kármán street. The plot also captures the downstream diffusion of this momentum jet as viscous effects widen the wake profile.

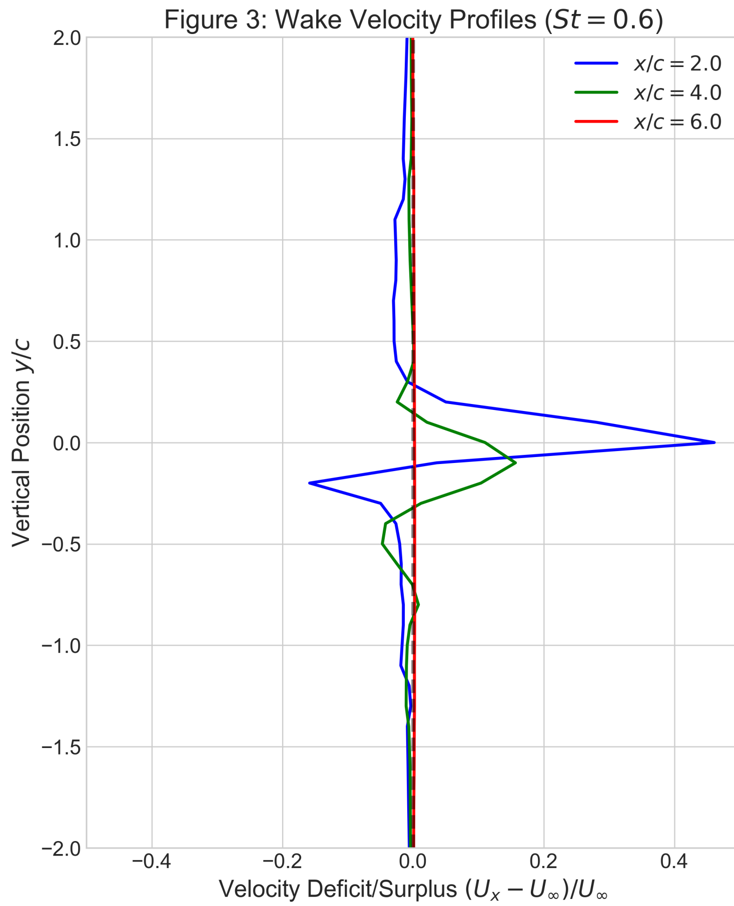

Figure 9: Instantaneous Wake Velocity Profiles at various downstream locations ($St = 0.6$).

3.3 Propulsive Efficiency and Wake Physics

A comprehensive parametric sweep was evaluated across six Strouhal numbers ranging from $St = 0.20$ to $St = 0.70$. Analysis of the mean thrust coefficient (C_{Tm}) confirms that the drag-to-thrust transition occurs near $St \approx 0.30$, above which the foil generates net positive forward thrust. The thrust coefficient increases monotonically with the Strouhal number, reaching $C_{Tm} = 0.3564$ at $St = 0.70$, reflecting the stronger transverse velocity signature. Concurrently, the RMS lift coefficient increases from 0.0929 at $St = 0.20$ to 2.4902 at $St = 0.70$. These trends are presented in Figure 10.

Figure 10 presents the propulsive performance metrics across the Strouhal range for our present study. The propulsive efficiency (η_p) is computed from the ratio of useful thrust power to total input oscillatory power for cases that contain the `propulsivePower` function object output ($St = 0.4, 0.5, 0.6, 0.7$). The efficiency peaks at $St = 0.6$ with $\eta_p = 49.18\%$ and slightly decreases to 47.74% at $St = 0.7$, displaying the characteristic "hump" curve. This peak efficiency is higher than the reference paper's linear amplitude case ($\approx 36.5\%$) because our quadratic amplitude envelope restricts bending to the posterior portion of the foil, reducing lateral fluid recoil and lowering the input power required for undulation.

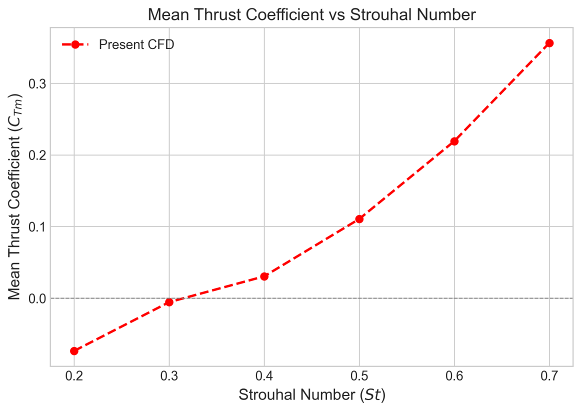

(a) Mean thrust coefficient C_{Tm}

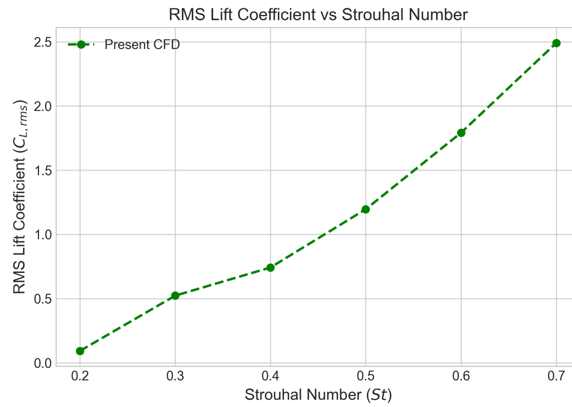

(b) RMS lift coefficient $C_{L,rms}$

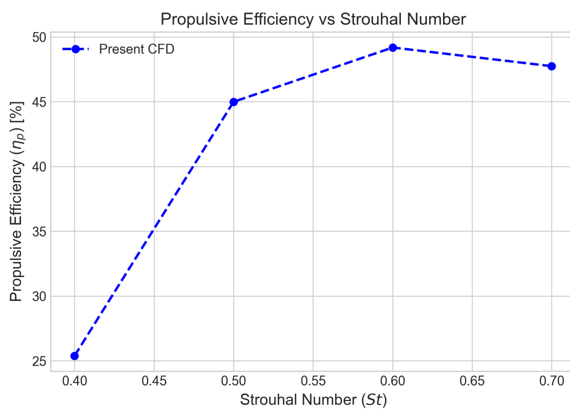

(c) Propulsive efficiency η_p

Figure 10: Parametric performance trends of the present undulating NACA0012 hydrofoil study for $\lambda^* = 0.8$: (a) Mean thrust coefficient (C_{Tm}), (b) RMS lift coefficient ($C_{L,rms}$), and (c) Propulsive efficiency (η_p).

Table 2: Parametric Performance Summary of the Undulating Hydrofoil ($\lambda^* = 0.8$)

St	Mean Thrust Coefficient (C_{Tm})	RMS Lift Coefficient ($C_{L,rms}$)	Propulsive Efficiency (η_p) [%]
0.20	−0.0737	0.0929	N/A
0.30	−0.0056	0.5231	N/A
0.40	+0.0304	0.7424	25.38
0.50	+0.1106	1.1958	44.99
0.60	+0.2192	1.7910	**49.18**
0.70	+0.3564	2.4902	47.74

N/A: Propulsive efficiency requires input power data (`propulsivePower` function object). Drag-producing cases ($St \leq 0.3$) do not generate net thrust.

4 Conclusions

This study demonstrated the use of the Overset (Chimera) Mesh framework in OpenFOAM-v2412 for numerical simulation of undulatory propulsion. The following key findings were established from the simulation data:

- The drag-to-thrust transition is captured near $St \approx 0.30$, confirmed by the sign change in C_{Tm} from -0.0056 at $St = 0.30$ to $+0.0304$ at $St = 0.40$.
- The propulsive efficiency, computed from the `propulsivePower` function object, peaks at $\eta_p = 49.18\%$ for the $St = 0.6$ case and slightly decreases to 47.74% at $St = 0.7$, consistent with the expected "hump" efficiency behaviour of bio-inspired undulatory propulsion.
- Instantaneous vorticity contours confirm the classical wake topology transition: a drag-producing standard von Kármán street at $St = 0.2$ evolves into a thrust-producing Reverse von Kármán street at $St = 0.6$, generating a strong centerline propulsive jet with $|U| > 1.2$ m/s.

5 Acknowledgement

This project was carried out as part of the FOSSEE Semester-Long Internship 2026. The author would like to thank the FOSSEE team at IIT Bombay for their support and resources.

References

[1] N. Thekkethil, A. Sharma, and A. Agrawal, "Unified hydrodynamics study for various types of fishes-like undulating rigid hydrofoil in a free stream flow," *Physics of Fluids*, vol. 30, no. 7, p. 071901, 2018.

A Key OpenFOAM Dictionary Files

A.1 Dynamic Mesh Dictionary (dynamicMeshDict)

The undulatory motion is prescribed via a coded solver in dynamicMeshDict. The frequency parameter f is the only variable changed between parametric cases.

```
dynamicFvMesh       dynamicOversetFvMesh;
libs                (overset fvMotionSolvers);
solver              coded;
name                prescribedUndulation;

code
#{
    // Undulation parameters
    const scalar f = 3;          // Hz  -- changes per St case
    const scalar omega = 2*pi*f;
    const scalar k = 2*pi/0.8;  // reduced wavelength lambda*=0.8
    const scalar c0=0.02, c1=-0.08, c2=0.16;
    // Amplitude envelope: A(x)=c0+c1*x+c2*x^2 => 0.10 m at x=1

    const scalar ramp = min(1.0, t/0.1); // 0.1 s startup ramp
    // ... (point motion loop with overset zone & falloff logic)
#};
```

A.2 Control Dictionary (controlDict)

Key solver and function-object settings for the base $St = 0.6$ case:

```
application     overPimpleDyMFoam;
startFrom       latestTime;
endTime         3.0;        // 9 oscillation cycles at St=0.6
deltaT          0.001;      // 0.001 s (initially 0.0005 s)
writeControl    adjustable;
writeInterval   0.01;
purgeWrite      50;
writeFormat     binary;

functions {
    forces {
        type            forceCoeffs;
        patches         (foil);
        rho             rhoInf;  rhoInf 1;
        liftDir (0 1 0); dragDir (1 0 0);
        magUInf 1;  lRef 1;  Aref 0.1;
    }
    propulsivePower {
```

```
        type            forces;
        patches         (foil);
        force yes;  moment yes;  power yes;
        rhoInf 1.0;
    }
    vorticity {
        type            vorticity;
        libs            (fieldFunctionObjects);
        writeControl    writeTime;
    }
}
```

A.3 Domain Decomposition (`decomposeParDict`)

```
numberOfSubdomains 7;
method          scotch;
```

B Parametric Study Configuration

Table 3: Parametric Study Case Configuration ($U_\infty = 1.0\,\text{m/s}$, $\lambda^* = 0.8$, $\Delta t = 0.0005 \rightarrow 0.001\,\text{s}$)

Case	St	f [Hz]	T [s]	Steps/Cycle
st0.2	0.20	1.0	1.000	1000
st0.3	0.30	1.5	0.667	667
st0.4	0.40	2.0	0.500	500
st0.5	0.50	2.5	0.400	400
st0.6	0.60	3.0	0.333	333
st0.7	0.70	3.5	0.286	286